Reaction Chemistry & Engineering

ROYAL SOCIETY OF CHEMISTRY

PAPER

View Article Online
View Journal

Cite this: DOI: 10.1039/d6re00024j

Continuous microreactor synthesis of size-controlled Ru nanoparticles to probe support and size effects in ammonia cracking

Joseph El-Kadi and Laura Torrente-Murciano *

Received 15th January 2026,
Accepted 5th April 2026

DOI: 10.1039/d6re00024j

rsc.li/reaction-engineering

Decoupling support and size effects and revealing size–activity relationships remain key challenges in the design and understanding of heterogeneous catalysts, especially for structurally sensitive reactions such as ammonia cracking for the on-demand production of hydrogen. This study demonstrates a new strategy to achieve both objectives where ruthenium nanoparticles (Ru NPs) with specific sizes are synthesised in the absence of capping ligands in a bespoke continuous 3D microreactor prior to their immobilisation on a range of supports. By keeping constant the average Ru NP size (~2.5 nm), the study reveals the high activity of ceria and zirconia supports due to strong-metal support interaction-like behaviour, with ammonia cracking activities an order of magnitude higher than the Ru/carbon nanotubes benchmark catalyst. In addition, size–activity relationships of Ru NPs between 2.5 and 5.5 nm supported on nanostructured ceria corroborates the theoretical predictions of an increased activity as the particle size decreases within this range, associated to an increase in the density of 'B_5' active sites on Ru NPs. This work demonstrates the potential of size-controlled wet synthesis of nanoparticles to reveal fundamental knowledge for the design and understanding of heterogeneous catalysts while simultaneously providing new routes for their manufacture.

Introduction

Heterogeneous catalysts are currently used to produce more than 80% of all chemical products worldwide[1] and are poised to play a crucial role in the global energy transition, with applications in energy storage, harvesting, generation, and Power-X-Power technologies.[2] Many heterogeneous catalysts are conventionally prepared by impregnation methods where active sites, mainly in the form of metal nanoparticles, are synthesised directly on the surface of a support. Although impregnation methods are widespread, they normally lack control of the size, a key parameter determining the resulting catalytic activity. In addition, when using impregnation methods, the size of the nanoparticles is strongly dependent on the support used, preventing the ability to decouple both effects. Understanding the individual effects of the particle size and support is particularly relevant for structurally sensitive reactions where catalytic activity is strongly dependent on the metal nanoparticle size, usually below 10 nm.[3] Ammonia cracking (*i.e.* decomposition) for the production of hydrogen on-demand is an example of a structurally sensitive reaction that has recently gained attention[4–6] due to the potential of ammonia as a carbon-free energy vector,[7,8] as recognized by the International Energy Agency.[9] Ammonia overcomes issues associated with the transport and storage of hydrogen, and can be cracked to produce hydrogen for fuel cells or partially cracked to enable NO_x-free ammonia combustion.[10] The design of supported heterogeneous catalysts with precise nanoparticle sizes presented in this paper provides fundamental understanding to enable the optimisation of ammonia cracking.

For ammonia cracking catalysis, the most active metal is ruthenium,[11] an expensive, rare-earth metal. Theoretical studies identify 2–3 nm as the optimum size of Ru nanoparticles,[12–14] based on the maximisation of the density of 'B_5' active sites where the recombinative desorption of N adatoms (the rate limiting step at low temperatures, irrespective of the metal[15,16]) is believed to occur. The superior activity of ruthenium is explained by its optimum nitrogen binding energy; it does not bind to the nitrogen of the ammonia molecule too strongly or too weakly as per the Sabatier principle. On the other hand, experimental studies for ruthenium in ammonia cracking report conflicting size–activity trends[17–19] depending on the effect of the support, the nanoparticle shape, or altering the catalyst treatment temperature (in calcination and annealing), which affects both size and metal–support interactions. These size–activity studies are limited by the inability to independently control the nanoparticle size on various catalyst supports *via*

Department of Chemical Engineering and Biotechnology, University of Cambridge, Philippa Fawcett Drive, CB3 0AS, Cambridge, UK. E-mail: lt416@cam.ac.uk

traditional wet impregnation, which has prevented a fair investigation of the effect of different Ru supports and sizes.

Despite the high cost of Ru, it is still a primary choice for developing ammonia cracking technologies due to its ability to crack ammonia at significantly lower temperatures compared to other metals, owing to the optimal Ru–N binding energy.[20,21] This may result in an overall enhancement of system efficiency and cost. Furthermore, given the knowledge around the B_5 active sites and theoretical studies investigating the optimal size of Ru, it serves as a necessary starting point to understand the effect of the size on the reactivity and metal–support interaction, and the experimental methodologies herein can also be extended to investigate other non-noble metals.

The lack of metal NP size control has driven research into alternative catalyst synthesis methods such as co-precipitation, deposition precipitation, and ion adsorption, among others.[22–25] The colloidal synthesis of metal nanoparticles followed by their immobilisation (or deposition) onto supports is a relatively recent method of catalyst synthesis, which provides an opportunity to control the size. Separating the synthesis and immobilisation steps provides more size control compared to synthesising the NPs directly on the support. However, to date, size control has not been achieved in Ru NP colloidal synthesis unless stabilising ligands are used[26–30] with likely detrimental effects on the final catalytic applications.[31,32] On the other hand, our group had developed flow synthesis technology[32–35] to grow metal nanoparticles under laminar flow, in the absence of capping ligands, with the ability to manipulate fluid dynamics to tune average size.

In this work we present a new method for the synthesis of supported ruthenium-based catalysts with precise nanoparticle sizes on various supports, involving the flow synthesis and immobilisation of Ru nanoparticles in the absence of organic capping ligands. For the first time, a constant Ru NP size of ~2.5 nm has been supported on various materials, enabling the decoupling of size and support effects, revealing the high activity of ceria and zirconia supports. In addition, the Ru NP size was varied between 2.8 and 5.3 nm, which confirmed theory-predicted size–activity trends. The paper presents a new capability provided by the flow synthesis of nanoparticles with tuneable sizes and their post-synthesis deposition, to reveal fundamental knowledge and optimise catalysts for structurally sensitive reactions while potentially enabling routes for their manufacture.

Experimental section

Ruthenium nanoparticle and catalyst synthesis methods

Ruthenium nanoparticles (Ru NPs) were synthesised in a 3D micro-scale coiled flow inverter reactor (CFIR) *via* wet reduction of 2.5 mM ruthenium nitrosyl nitrate (1.5 w/v% in dilute nitric acid, Sigma Aldrich) with 6.25 mM sodium borohydride ($NaBH_4$, ~12 wt% in 14 M NaOH, Sigma-Aldrich). In a typical synthesis (Fig. 1), aqueous solutions of ruthenium nitrosyl nitrate and alkaline sodium borohydride were fed at 115 mL h^{-1} each, using syringe pumps into a 0.02 inch T-mixer. The helical geometry of the CFIR promotes secondary Dean flows, ensuring a mixing time of <50 ms, which is critical for achieving narrow size distributions in the absence of organic capping agents. The resulting colloidal suspension was quenched with 0.1 M HNO_3 to decompose excess $NaBH_4$ and stabilize the particles for subsequent support loading. A more exhaustive characterization of this specific reactor's fluid dynamics and the chemical mechanism of the ruthenium nitrite complex is provided in detail and our previous study cited herein.[35]

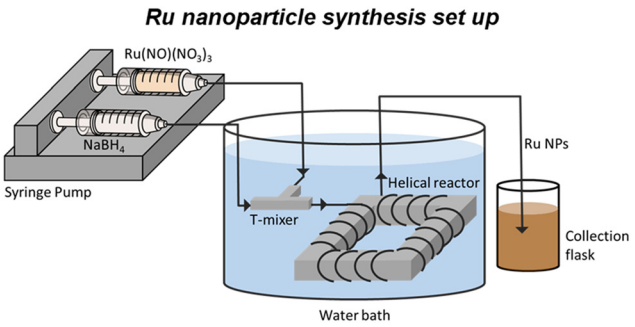

Fig. 1 Ru nanoparticle continuous reactor set up: two syringe pumps control flow rates of $Ru(NO)(NO_3)_3$ and $NaBH_4$ solutions. Reactants were mixed with a T-mixer in crossflow configuration and the resulting solution passes through the coiled flow inverter reactor (CFIR), before collection in nitric acid solution at an outlet for electrostatic stabilisation prior to immobilisation on a support.

To immobilise the Ru NPs onto a support, colloidal Ru NPs were collected from the outlet of the flow reactor in 1 M nitric acid (HNO_3, Fisher Scientific) for electrostatic stabilisation.[35] After NP collection, a support was added, and the suspension was magnetically stirred at 500 rpm for 30 min. The liquid was removed from the suspension by rotary evaporation, and the catalyst was dried at 80 °C under <100 mbar vacuum overnight and then calcined in air at 250 °C for 2 h with a 2 °C min^{-1} ramp. The resulting catalyst was washed again with 40 mL DI water through a vacuum filter with a membrane (nylon 66, 0.2 micron pore size, 47 mm diameter, Supelco) to remove remnant nitrates, sodium, and boron from the precursors, followed by drying again at 80 °C under <100 mbar vacuum overnight. Mesoporous carbon (mesoC, ACM), ceria nanopowder (CeO_2, 99.5%, Alfa Aesar) zirconia (ZrO_2, Johnson Matthey), alumina (Al_2O_3, Puralox, Johnson Matthey) and carbon nanotubes (CNT, Nanocyl) were used as supports, as well as ceria nanorods (CeO_2-NRs), nanoparticles (CeO_2-NPs), and nanocubes (CeO_2-NCs) prepared hydrothermally as described elsewhere.[36]

To decrease the average Ru NP size, the T-mixer diameter of the flow synthesis reactor was decreased from 0.02 inch to 0.01 inch, after which the collected Ru NPs were immobilised on ceria nanopowder following the same procedure as above. To increase the average Ru NP size on the ceria nanopowder support, wet impregnation and incipient wetness

impregnation preparation methods were employed. In the wet impregnation method, 0.13 g of support and 50 mL of 1.25 mM $Ru(NO)(NO_3)_3$ were mixed at 500 rpm for 30 min, followed by liquid removal by rotary evaporation, drying, calcination, washing and drying under the same conditions as for the flow-synthesised catalysts. In the incipient wetness impregnation, $Ru(NO)(NO_3)_3$ was diluted in DI water to the volume corresponding to the support's pore volume and added dropwise to the support, followed by the same drying and calcining conditions as for the flow-synthesised catalysts. For comparison to the literature, a benchmark 7 wt% Ru/CNT catalyst was also prepared *via* incipient wetness impregnation of $Ru(NO)(NO_3)_3$.

Catalyst characterisation

Transmission Electron Microscopy with a Talos FEI microscope (200 kV) was used to determine average supported Ru NP size. For the sample preparation, a few milligrams of powdered catalyst were suspended in 3 mL ethanol and sonicated for 10 min in an ultrasonication bath, after which 3 μL were drop casted onto a carbon-coated copper TEM grid (400 mesh, Agar Scientific) and left to dry at room temperature for at least 1 h. For samples with poor contrast between Ru and the support in TEM, either the lattice spacing of hexagonal close-packed Ru(0) metal of 0.22 nm (ref. 37 and 38) was used to locate Ru NPs or the High-Angle Annular Dark-Field Imaging in Scanning Transmission Electron Microscopy (STEM) mode was conducted. For each imaged sample, a particle size distribution histogram was constructed using ImageJ open-source software from at least 3 images taken from different mesh sections of the TEM grid.

Inductively Coupled Plasma-Mass Spectrometry (ICP-MS) was used to determine the Ru weight loading of the flow-synthesised Ru catalysts using a Thermo-Fisher Nexion 2000-S machine. 10 mg of the catalyst sample was added to 2 mL of *aqua regia* prepared by mixing nitric acid (70%, Fisher Scientific) and hydrochloric acid (37%, Acros Organics) in a 1 : 3 volume ratio, respectively. Ru was digested by heating the solution to 80 °C in an enclosed water bath for 12 h and diluted to 15 mL to prepare a stock solution. Then, 0.5 mL of stock solution was diluted twice, each time with the addition of 0.25 mL of HNO_3 (67–69%, Normatom) to avoid reprecipitation of the Ru species, to produce a final dilution factor of 15 000, with analyses conducted in triplicates. The digestion of ruthenium is a challenge that is subject of extensive research,[39] thus an uncertainty of ±30% in the final loading value is considered based on tests on reference samples.

Hydrogen temperature programmed reduction (TPR) experiments were conducted in a Micromeritics Autochem II 2920 apparatus equipped with a mass flow-controlled gas manifold and thermal conductivity detector (TCD). 20–50 mg of sample were placed in a quartz flow reactor located within a programmable furnace and subjected to 50 sccm 5% H_2/Ar (BOC). The reactor temperature was increased from ambient temperature to 900 °C at a ramp rate of 10 °C min^{-1}. Carbon monoxide (CO) chemisorption experiments were conducted in the Micromeritics Autochem II 2920 apparatus. 20–50 mg of catalyst were first reduced in 50 sccm 5% H_2/Ar (BOC) at 300 °C for 0.5 h before cooling to 40 °C under 50 sccm Ar. Then a controlled volume (~0.5 cm^3) of 5% CO/He (BOC) was pulsed through the sample with 50 sccm He carrier gas.

Catalyst testing

Ammonia cracking reactions were carried out in a bespoke rig in a continuous packed bed reactor with a gas hourly space velocity of 6000 mL_{NH_3} g_{cat}^{-1} h^{-1} with 25 mg of the catalyst in a silicon carbide bed. The reactor system was equipped with mass flow and temperature controllers. During each catalytic study, the reaction temperature was ramped up and down between 200 °C to 500 °C at a rate of 2.6 °C min^{-1} three times using a Carbolite tubular furnace with PID control. The reactor exit gas was analysed using an on-line gas chromatography fitted with a Porapak Q column and thermal conductivity detector. Prior to testing, catalysts were reduced *in situ* using 10 sccm H_2 at 300 °C for 0.5 h with a ramp rate of 5 °C min^{-1}.

Conversion was calculated based on H_2 production measured by gas chromatography considering the variation in the number of moles, with activity onset considered above 5% ammonia conversion based on instrument error. Activation energy, E_a, was calculated as an average from Arrhenius plots of the three temperature cycles in the range of 5–20% conversion. The catalytic activity is compared using the T_5, which is defined as the temperature at which 5% ammonia conversion is achieved under the specified gas hourly space velocity (GHSV). This metric serves as a proxy for the 'light-off' temperature and allows for a comparison of the temperature of intrinsic activity of the catalysts at low conversion levels, minimizing the influence of equilibrium limitations.

Results and discussion

Decoupling size–support effects

To decouple, for the first time, the size and support effects on Ru-based catalysts, a constant Ru NP size of ~2.5 nm was selected based on the optimum ~2–3 nm size range identified by theoretical studies[12–14] based on the maximisation of the density of 'B_5' active sites. Colloidal Ru NPs were synthesised in a coiled flow inverter reactor in the absence of capping ligands and supported on a range of supports by post-synthesis impregnation or 'immobilisation'. These catalysts are denoted as Ru/*S* where *S* is the different support: mesoC (mesoporous carbon), ZrO_2 (zirconia), Al_2O_3 (alumina), CeO_2-NR (ceria nanorods), CeO_2-NP (nanoparticles), CeO_2-NC (nanocubes), and CNT (carbon nanotubes). A reference 'benchmark' Ru/CNT catalyst was also prepared and denoted '7wt% Ru/CNT IWI' to indicate its 7% weight loading and the incipient wetness impregnation (IWI) method of preparation. This catalyst was selected for reference as it is well-accepted in the literature that CNT

facilitates the formation of optimum ~2–3 nm Ru NPs *via* impregnation leading to a high ammonia cracking activity.[5,40] While the flow-synthesised catalysts demonstrate significantly higher turnover frequencies than the 7 wt% Ru/CNT benchmark, it is important to note that the 7 wt% Ru/CNT IWI catalyst serves as a high-loading conventional reference point rather than a direct structural analogue. Due to differences in the synthesis and Ru loading, the observed order-of-magnitude difference in the activity is intended to highlight the high efficiency of the flow-immobilization strategy at low loadings, though a direct intrinsic comparison is limited by these differing preparation histories.

TEM images and catalytic performance results are presented in Fig. 2 and key information on the catalysts is summarised in Table 1. Complete three-cycle catalyst testing plots can be found in SI Fig. S1. In this case, all catalysts are also stable after three consecutive cycles under temperature ramping conditions between 200 and 500 °C. It is believed that this high thermal stability and activity of these catalysts is related to the strong metal–support interaction-like behaviour promoted by the calcination step at 250 °C. In the absence of this calcination step, the Ru NPs are easily removed during the washing step in the preparation, leading to a low metal loading.

The TEM characterisation of the different catalysts (Fig. 2a) demonstrates that the preparation method is capable of supporting Ru NPs in a range of supports while keeping the original colloidal sizes. All the catalysts showed an average support Ru NP size of ~2.5 nm, within standard deviations of each other, except for Ru/CNT, which shows a slight decrease in the Ru NP size to 1.7 nm, likely an artifact of microscopy characterisation in curved supports. The stable catalytic activity in consecutive cycles, as shown in Fig. S1, suggests that that there is no sintering occurring under reaction conditions within the temperature range considered.

Decoupling the size–support effects on ammonia cracking offers interesting insights into the roles of the support in the ammonia cracking reaction. Ceria supported catalysts, independent of their nanostructure morphology (such as nanoparticles, nanorods or nanocubes) present an onset of catalytic activity at lower temperatures (~295–300 °C, denoted the T_5 value), and a lower activation energy of ~91 kJ mol^{-1} compared to the other catalysts, which display values above 100 kJ mol^{-1}. The low temperature activity of the Ru/CeO_2 catalysts may be related to the electronic promotion of the Ru active sites by the ceria support,[6] enabling N_2 recombination, which is the rate limiting step under these conditions.[15,16] This approach also enables the decoupling of size–morphology effects for a given support, in this case ceria. Ru/CeO_2-nanoparticles and Ru/CeO_2-nanocubes catalysts display ~1.7× the turnover frequency (TOF) of Ru/CeO_2-nanorods at 375 °C (Fig. 2c). Although 1D supports such as ceria nanorods are known to present high catalytic activities due to the strain created by the curved support on the nanoparticles,[6] ceria nanocubes do not normally lead to good catalysts *via* impregnation due to their high hydrophobicity and low surface area, resulting in large metal nanoparticles. These new insights demonstrate that ceria nanocubes do indeed present a strong metal–support interaction-like behaviour and as a result, high activity in ammonia cracking, when metal nanoparticle size is properly controlled.

Comparing all the different supports in this study, zirconia presents a remarkable activity, >30% higher than any other support, with a turnover frequency of 1600 mol_{H_2} mol_{Ru}^{-1} h^{-1} at 375 °C, ~16× that of the benchmark 7 wt% Ru/CNT IWI catalyst (Fig. 2c). It is interesting to note that the onset temperature T_5 is higher (331 °C) than those of ceria-based supports, which may be due to the weaker support electron-donating properties of ZrO_2 compared to CeO_2. The higher hydrogen consumption per mole of Ru NPs on the ZrO_2, CeO_2-nanoparticles and CeO_2-nanocubes supports (Table 1) may also be related to a strong metal–support interaction-like behaviour. While H_2-TPR and hydrogen consumption data are suggestive of strong interaction-like behaviour, we acknowledge these bulk observations do not provide direct spectroscopic evidence of electronic shifts. Therefore, the observed performance is referred to as 'strong interaction-like behaviour,' as further *in situ* characterization would be required to definitively decouple interfacial electronic promotion from geometric effects.

The hydrogen consumption for Ru on ZrO_2, CeO_2-nanoparticles and CeO_2-nanocubes is above the theoretical stoichiometric value of 2 assuming that the Ru NPs have been fully re-oxidised in the calcination step. Such strong interaction-like behaviour between Ru and ZrO_2, CeO_2-nanaoparticles and CeO_2-nanaocubes may support the simultaneous reduction of the supports at low temperatures, perhaps due to H_2 spill-over from Ru into the support during the reduction, which potentially promotes the formation of active sites at the interface of the metal and support with extraordinary catalytic activity.[41,42] As seen in the H_2 temperature programmed reduction plots (Fig. 3), the enhanced reduction of Ru supported on ZrO_2 and CeO_2 supports below 300 °C, coupled with the above theoretical stoichiometric values of hydrogen consumption noted in Table 1, may suggest the strong metal–support interaction-like behaviour between Ru and these supports. Furthermore, in this study, TOFs are normalized to total Ru loading to provide a consistent basis for comparison; however, we acknowledge this does not account for variations in surface-exposed Ru atoms. While a ~30% uncertainty in Ru loading exists due to digestion challenges in ICP-MS, the performance gap between the most active catalysts (Ru/ZrO_2 and Ru/CeO_2) and the benchmarks is sufficiently large (up to 16×) that the relative activity rankings remain robust despite these loading uncertainties.

Interestingly, alumina, another metal oxide support, does not show high activity. In this case, a clear Ru reduction peak is observed in the TPR analysis of the Ru/Al_2O_3 catalyst at 139 °C with relatively small H_2 consumption, indicating poor metal–support interaction and consequently low activity. For

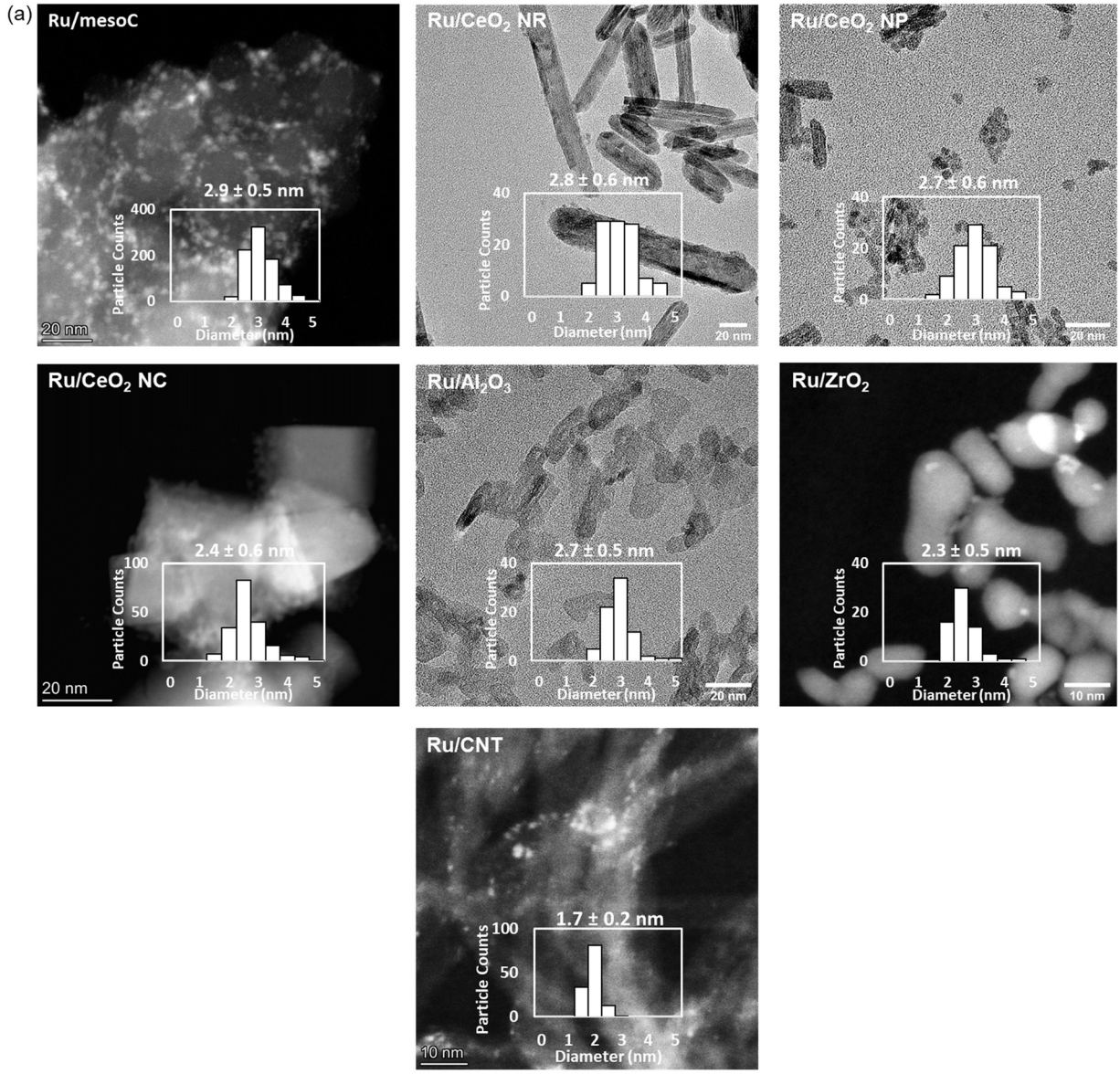

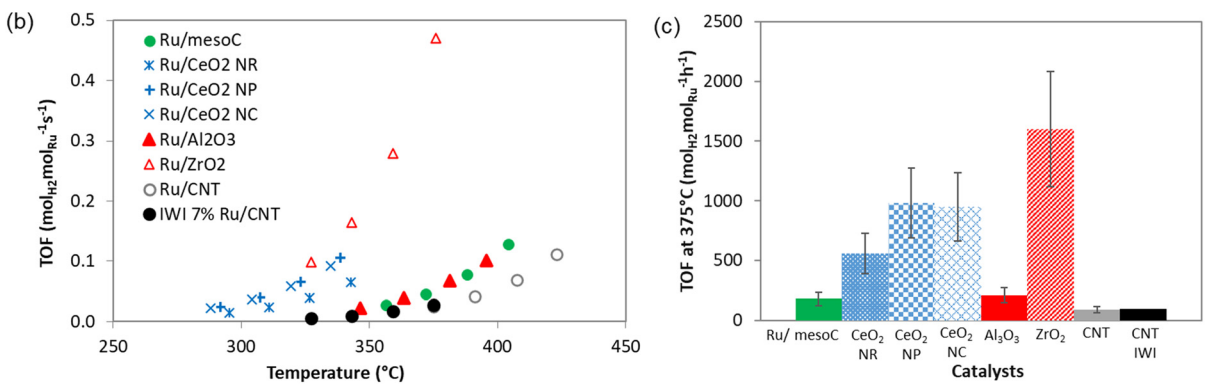

Fig. 2 (a) Representative TEM images with particle size histograms for Ru/*S* catalysts, prepared by immobilising flow-synthesised Ru NPs on various supports – information on catalysts are in Table 1. (b) Ammonia cracking turnover frequency rates *versus* temperature in the range of 5–20% conversion. (c) Turnover frequency rates at 350 °C plotted against average supported Ru NP size from TEM. Vertical error bars for flow-synthesised catalysts represent maximum error (±30%) in Ru loading determination from digested catalysts with ICP-MS. Graph display data for second temperature ramp cycle (out of three) in a packed bed reactor with GHSV of 6000 mL_{NH_3} g_{cat}^{-1} h^{-1}; 2.5 sccm NH_3 with 5 sccm He; 25 mg of catalyst dispersed in 450 mg of inert SiC; catalysts reduced *in situ* prior to testing with 10 sccm H_2 at 300 °C for 0.5 h, 5 °C min^{-1} ramp. Complete three-cycle catalyst testing plots can be found in SI Fig. S1. Complete TEM images showing locations of supported Ru NPs can be found in Fig. S3.

Table 1 Ru/*S* catalysts prepared by immobilising flow-synthesised Ru NPs on various supports, including resulting average supported Ru NP size under TEM, Ru loading from digested catalysts and catalytic performance data

Catalyst	Size of immobilised Ru NPs from TEM (nm)	Number of particles counted	H_2 consumption in H_2-TPR (mol_{H_2} mol_{Ru}^{-1})	Ru loading (wt%)	Catalyst performance: Turnover frequency at 375 °C (mol_{H_2} mol_{Ru}^{-1} h^{-1})	Activation energy (kJ mol^{-1})	Temperature for 5% NH_3 conversion (T_5 value)
Ru/mesoC	2.9 ± 0.5	856	4.1	2.2	180	115 ± 1	355
Ru/CeO_2-NR	2.8 ± 0.6	90	6.4	3.3	560	92 ± 3	299
Ru/CeO_2-NP	2.7 ± 0.6	103	12.6	2.0	980	91 ± 2	295
Ru/CeO_2-NC	2.4 ± 0.6	191	13.6	2.0	950	90 ± 6	294
Ru/Al_2O_3	2.7 ± 0.5	77	6.3	2.1	210	105 ± 1	350
Ru/ZrO_2	2.3 ± 0.5	65	16.2	0.5	1600	105 ± 1	331
Ru/CNT	1.7 ± 0.2	129	9.3	2.4	90	121 ± 4	374
7 wt% Ru/CNT IWI	2.8 ± 0.9	276	4.2	7[a]	100	105 ± 2	335

[a] Assumed based on impregnated quantity of Ru.

comparison purposes, our previous studies on cobalt NPs supported on alumina demonstrate the formation of irreducible aluminates when the metal–support interaction is strong with poor catalytic activity.[43] Finally, Ru-based carbon-based supports (mesoporous carbon and carbon nanotubes) show comparably low catalytic activities towards ammonia cracking. Both Ru/CNT samples prepared by impregnation of pre-synthesised Ru NPs and incipient wetness impregnation have very similar activities with turnover frequencies of 90–100 mol_{H_2} mol_{Ru}^{-1} h^{-1} at 375 °C. It is interesting to point out that the hydrogen consumption during TPR analysis of these catalysts is lower than the most active catalysts in the study.

Ruthenium NP size–activity relationship on ammonia cracking

Understanding the intrinsic size–activity relationship of Ru for the ammonia cracking reaction was demonstrated by preparing colloidal Ru NPs of different sizes in flow and supporting them on the CeO_2 nanopowder support. Colloidal Ru NPs were prepared in a coiled flow inverter reactor in the absence of capping ligands, where the degree of mixing in the T-mixer (where the Ru precursor and reducing agent meet) was found to have a key effect on the resulting size.[35] The colloidal NPs were electrostatically stabilised with nitric acid followed by immobilisation on the CeO_2 support, producing average supported Ru NP sizes of 2.8 nm and 3.6 nm with a 0.01 inch and 0.02 inch T-mixer, respectively. Attempts to increase the average size by further increasing the diameter of the T-mixer were not successful as they led to agglomeration of the particles. Instead, the average Ru size was then increased to 4.3 nm and 5.3 nm *via* wet and incipient wetness impregnation, respectively. Similar size distributions between ±0.8–1 nm were obtained in all syntheses.

The catalysts of Ru supported on CeO_2 are denoted by *X* nm Ru/CeO_2, where *X* is the average Ru NP size in nanometres determined from TEM. TEM images and catalytic performance results are presented in Fig. 4 and key information on the catalysts is summarised in Table 2. As the average supported Ru NP size decreases from 5.3 nm to 2.8 nm, the turnover rate of ammonia cracking increases by around twofold from 220 to 450 mol_{H_2} mol_{Ru}^{-1} s^{-1} at 350 °C and the average activation energy decreases from 98 kJ mol^{-1} to 89 kJ mol^{-1}, respectively (Fig. 4, Table 2). The observed differences between TEM and CO chemisorption arise because TEM measures the physical diameter of the primary particles, while CO chemisorption measures the accessible metallic surface area. Variations in the size sequence for CO data likely stem from metal–support interactions, where the support may partially decorate the Ru surface.[44] Complete three-cycle catalyst testing plots can be found in SI Fig. S2. All catalysts are stable after three consecutive cycles under temperature ramping conditions between 200 and 500 °C.

The catalytic activity, measured in moles of H_2 produced per mole of metal per hour of the Ru/CeO_2 catalysts, seems to increase exponentially as the Ru NP average size decreases (Fig. 4c). This seems to be in agreement with the theoretical predictions for the maximum density of B_5 active sites at a hemispherical Ru NP size of ~2–3 nm,[12–14] however, there is no indication that activity will drop at smaller Ru particles sizes <2.5 nm. It is possible that confinement effects at smaller particle sizes <2.5 nm are equally or more important than the formation of B_5 sites. Similar studies scattered in the literature, which attempt to vary the Ru particle size, involve the use of different Ru precursors,[45] varying support annealing temperature,[17] or varying catalyst reduction and calcination temperatures[18,46] which also have an impact on the metal–support interaction. Having said this, in general, our data agrees with other observations in the literature such as those by Zheng *et al.*[19] who experimentally demonstrated an increase in the TOF as the Ru particle size decreased from 4.6 to 2.2 nm on the Ru/Al_2O_3 catalyst.

The H_2 temperature programmed reduction plots for the *X* nm Ru/CeO_2 catalysts are presented in Fig. 5. Considering that all the catalysts were calcined in air at 250 °C during their preparation, Ru can be assumed to have been fully oxidised prior to H_2 TPR. While the theoretical stoichiometric reduction of RuO_2 to Ru involves 2 moles of H_2 per mol of Ru, the hydrogen consumption during TPR was considerably higher in all cases. In addition, the H_2 consumption of these catalysts per mole of ruthenium increases as the particle size decreases with

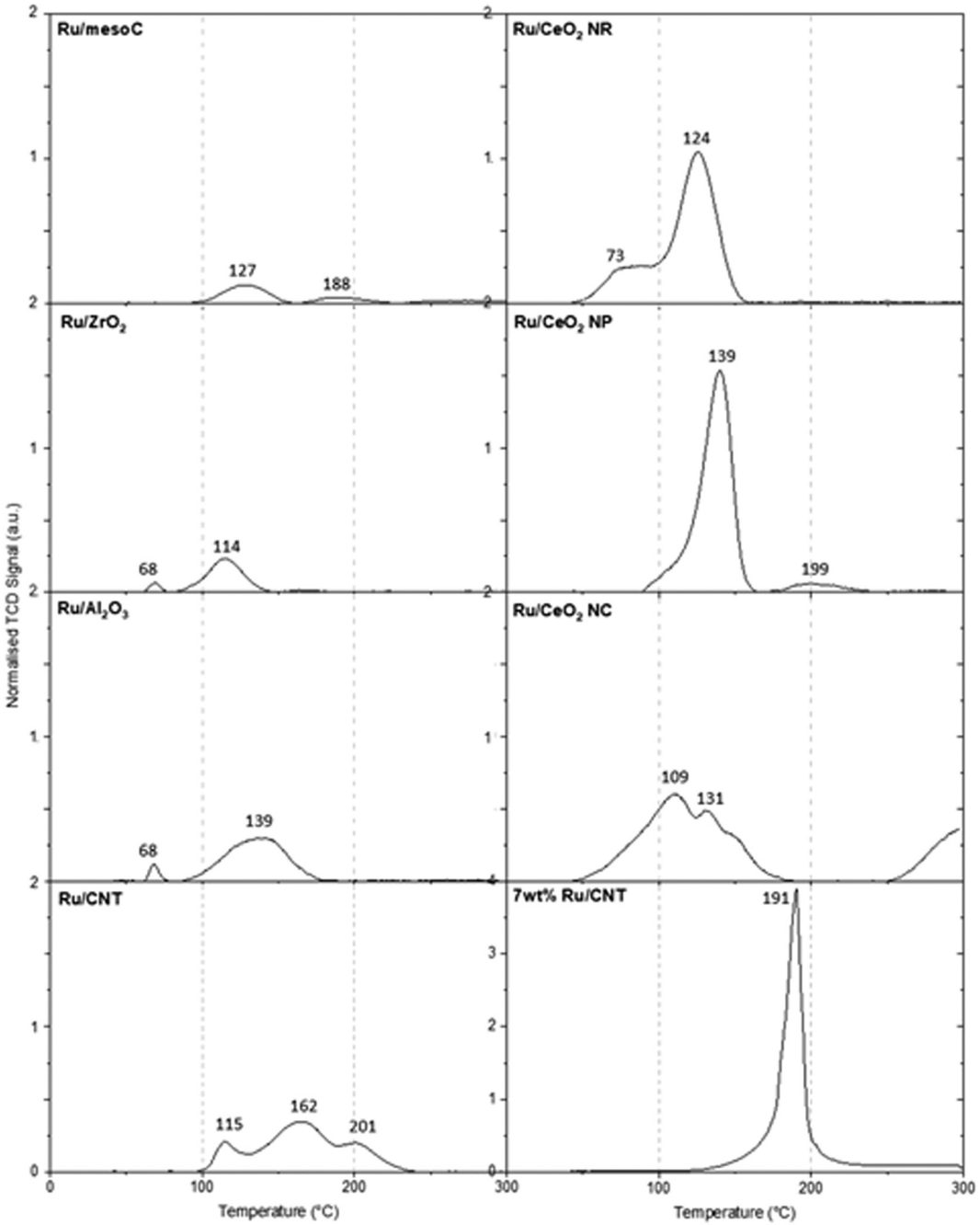

Fig. 3 H_2 TPR plots normalised by the mass of sample for various catalysts prepared by immobilising flow-synthesised Ru NPs – details of catalysts are in Table 1. Tests conducted with 50 mg of catalyst and 30 sccm of 5% H_2/Ar mixture; reactor temperature was increased from ambient temperature to 300 °C at a ramp rate of 10 °C min^{-1}. Note the change in the *y*-axis scale (TCD signal normalised by mass of sample) for the 7 wt% Ru/CNT catalyst due to the difference in weight loading of the catalyst.

a twofold increase from 6.7 to 13.0 mol_{H_2} mol_{Ru}^{-1} as the average Ru size decreases from 5.3 to 2.8 nm, suggesting an increase in hydrogen spill-over and ceria support reduction as the Ru size decreases. These graphs show the appearance of a shoulder at lower temperatures for the catalysts prepared by flow synthesis, which can be explained by the ease of reduction of the smaller nanoparticles.[47] The incipient and wet impregnated Ru/CeO_2 catalysts demonstrate larger relative peak areas, as expected due to higher achieved Ru loadings and the reduction of additional residual nitrates from the impregnated $Ru(NO)(NO_3)_3$ precursor.[48]

It is important to note that the synthetic method employed significantly influences not only the incorporation pathway of the metal precursor but also the resulting metal–support interactions and nanoparticle characteristics, including size distribution and crystallinity. While our study primarily attributes differences in catalytic activity to the Ru nanoparticle size, this is inherently linked to the method of incorporation.

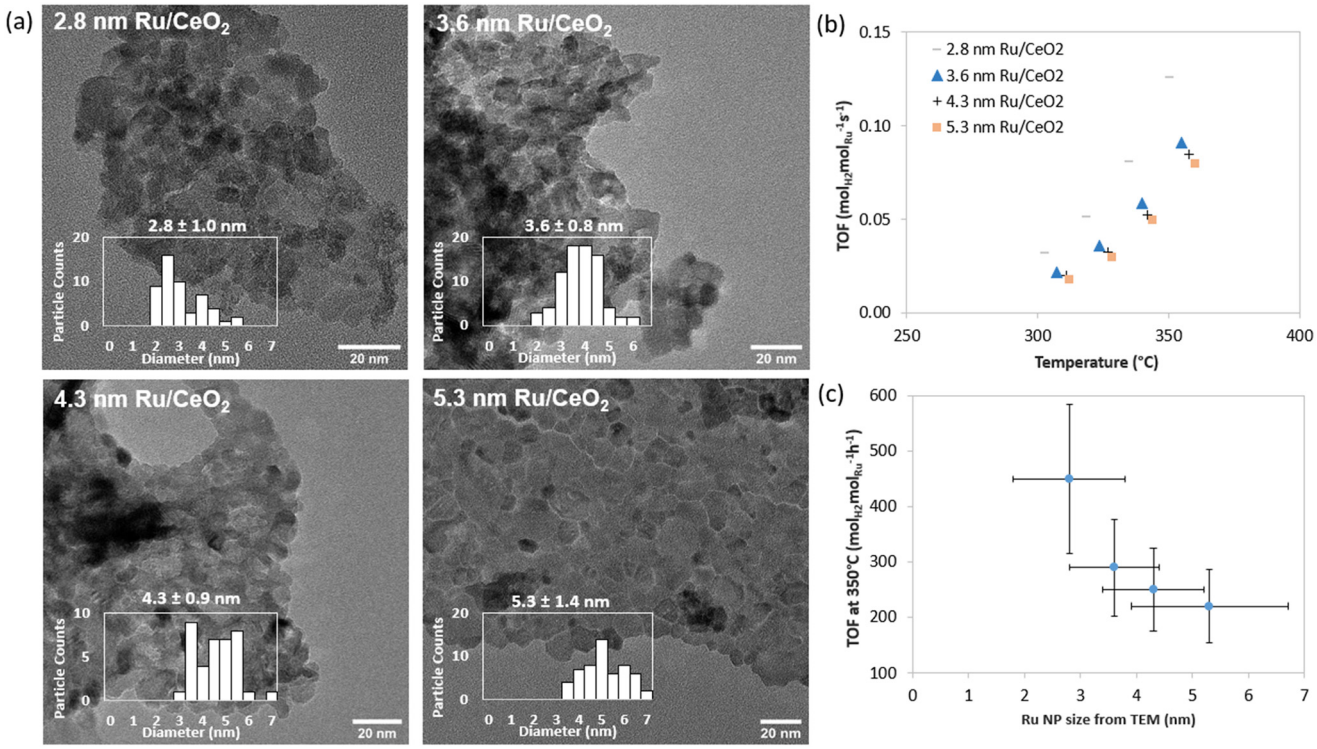

Fig. 4 (a) Representative TEM images with particle size histograms of *X* nm Ru/CeO_2 catalysts, where *X* denotes the average Ru NP size determined from TEM in nm – information on catalysts are in Table 2. (b) Ammonia cracking turnover frequency rates *versus* temperature in the range of 5–20% conversion. (c) Turnover frequency rates at 350 °C plotted against the average supported Ru NP size from TEM. Vertical error bars for flow-synthesised catalysts represent maximum error (±30%) in Ru loading determination with ICP-MS and horizontal error bars represent standard deviation of average size from TEM. Graph display data for the second temperature ramp cycle (out of three) in a packed bed reactor with GHSV of 6000 $mL_{NH_3}\ g_{cat}^{-1}\ h^{-1}$; 2.5 sccm NH_3 with 5 sccm He; 25 mg of catalyst dispersed in 450 mg of inert SiC; catalysts reduced *in situ* prior to testing with 10 sccm H_2 at 300 °C for 0.5 h, 5 °C min^{-1} ramp. Complete three-cycle catalyst testing plots can be found in SI Fig. S2. Complete TEM images showing locations of supported Ru NPs can be found in Fig. S3.

Table 2 Catalysts with different average Ru sizes prepared by immobilising flow-synthesised Ru NPs onto commercial nanopowder CeO_2 and impregnation, denoted as *X* nm Ru/CeO_2 where *X* is the average Ru NP size from TEM in nm

Catalyst	Synthesis method	Size of supported Ru NPs from TEM (nm)	Number of particles counted	H_2 consumption in H_2-TPR ($mol_{H_2}\ mol_{Ru}^{-1}$)	Average size of supported Ru NPs from CO chemisorption (nm)	Ru loading (wt%)	Catalyst performance	
							Turnover frequency at 350 °C ($mol_{H_2}\ mol_{Ru}^{-1}\ h^{-1}$)	Activation energy[a] (kJ mol^{-1})
2.8 nm Ru/CeO_2	Flow synthesis with 0.01″ T mixer	2.8 ± 1.0	26	13.0	1.6	1.4	448	89 ± 3
3.6 nm Ru/CeO_2	Flow synthesis with 0.02″ T mixer	3.6 ± 0.8	50	8.3	2.9	2.3	290	92 ± 1
4.3 nm Ru/CeO_2	Wet impregnation	4.3 ± 0.9	92	7.6	2.0	2.4	248	97 ± 2
5.3 nm Ru/CeO_2	Incipient wetness impregnation	5.3 ± 1.4	79	6.7	2.8	3.3	219	98 ± 1

[a] Calculated from Arrhenius plots from three successive temperature ramp cycles.

Ruthenium introduced *via* impregnation techniques, whether wet or incipient, typically forms metallic Ru in the hexagonal close-packed (hcp) crystal structure, with a characteristic lattice spacing of approximately 0.21 nm, as reported in the literature and confirmed in our study.[49] The face-centered cubic (fcc) phase of Ru is exceedingly rare and has only been observed under specific conditions involving stabilizers or ligands during synthesis,[50] which are not applicable in our case, as no such additives were used.

Interestingly, our observations showed that wet impregnation resulted in slightly smaller Ru particles than incipient wetness impregnation. This can be rationalized based

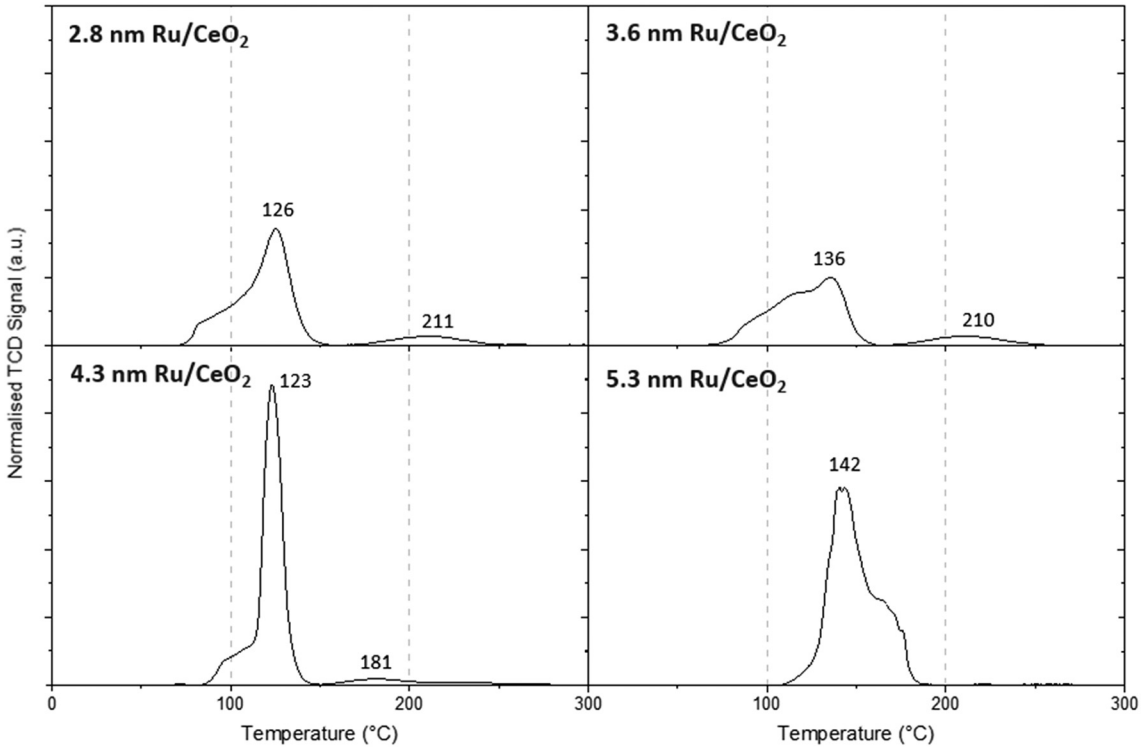

Fig. 5 H_2 TPR plots normalised by the mass of sample for Ru/CeO_2 catalysts – details of catalysts are in Table 2. Tests conducted with 50 mg of catalyst and 30 sccm of 5% H_2/Ar mixture; reactor temperature was increased from ambient temperature to 300 °C at a ramp rate of 10 °C min^{-1}.

on the distribution dynamics of the precursor solution: in wet impregnation, the support is fully immersed, allowing for a more homogeneous dispersion of the metal precursor across the surface. This often leads to improved dispersion and smaller particle sizes.[51] In contrast, incipient wetness impregnation involves the addition of a minimal volume of solution, just sufficient to fill the pore volume of the support, which may lead to localized precursor concentration and subsequent formation of larger or more agglomerated particles.

Conclusions and outlook

A novel Ru nanoparticle flow synthesis and immobilisation strategy has been developed to prepare heterogeneous catalysts with well-defined Ru NP sizes in the absence of capping ligands on a range of supports, enabling the decoupling of support and size effects on catalytic ammonia cracking. By keeping the Ru average size constant at ~2.5 nm, CeO_2 and ZrO_2 were identified as superior supports compared to Al_2O_3, mesoporous carbon, and carbon nanotubes, due to their strong metal–support interaction-like behaviour, showing activities an order of magnitude higher than the Ru/CNT benchmark catalyst. This catalyst synthesis approach also revealed insights about the intrinsic role of nanostructured morphologies of ceria, demonstrating that CeO_2 nanocubes can achieve a strong metal–support interaction-like behaviour and high activities, similar to that of CeO_2 nanorods, particularly high at low temperatures ~300 °C. Previously, the high hydrophobicity and low surface area of CeO_2 nanocubes had prevented small metal sizes to be achieved using traditional impregnation methods, which was overcome with this approach. Finally, the average Ru size on nanopowder CeO_2 was varied by manipulating the fluid dynamics of early mixing in the flow synthesis set-up. As the average supported Ru size decreased from 5.3 to 2.8 nm, ammonia cracking catalytic turnover frequency increased by twofold and activation energy decreased from 98 to 89 kJ mol^{-1}. This agrees with theoretical studies, which predict a maximum density of B_5 sites for hemispherical Ru NPs at ~2–3 nm. Further work should focus on the synthesis of smaller Ru NPs as the current experimental work does not suggest a drop in their activity as theory predicts.

This study is the first demonstration of how flow chemistry and the immobilisation of colloidal nanoparticle suspensions can reveal size–activity and support–activity trends for structurally sensitive reactions, revealing fundamental knowledge to guide the design of catalysts. This flow synthesis and immobilisation strategy developed in this study, in the absence of capping ligands, serves as a starting point for other supported scarce metal catalysts, particularly in structure-sensitive reactions like Fischer–Tropsch synthesis or selective hydrogenation, where independent control over nanoparticle size and support chemistry is vital for optimizing catalytic activity and metal utilisation.

Conflicts of interest

On behalf of all authors, the corresponding author states that there is no conflict of interest.

Data availability

The supporting data has been provided as part of the supplementary information (SI). Supplementary information: Fig. S1, complete consecutive catalytic data for different Ru NPs supported on a variety of supports. Fig. S2, complete consecutive catalytic data for Ru NPs of different sizes supported on ceria. Fig. S3, complete TEM data of all the catalysts. See DOI: https://doi.org/10.1039/d6re00024j.

Acknowledgements

The authors greatly acknowledge the financial support from the UK Engineering and Physical Science and Research Council (grant numbers EP/V025759/1 and EP/X016757/1) and the Department of Chemical Engineering and Biotechnology at the University of Cambridge for JEK's PhD scholarship. For the purpose of open access, the author has applied a Creative Commons Attribution (CC BY) licence to any Author Accepted Manuscript version arising from this submission.

References

1 X. Hu and A. C. K. Yip, *Front. Catal.*, 2021, **1**, 667–675.
2 Y. N. Xia, H. Yang and C. T. Campbell, *Acc. Chem. Res.*, 2013, **46**, 1671–1672.
3 M. P. C. van Etten, B. Zijlstra, E. J. M. Hensen and I. A. W. Filot, *ACS Catal.*, 2021, **11**, 8484–8492.
4 T. Bell and L. Torrente-Murciano, *Top. Catal.*, 2016, **59**, 1438–1457.
5 A. K. Hill and L. Torrente-Murciano, *Appl. Catal., B*, 2015, **172**, 129–135.
6 Z. G. Hu, J. Mahin, S. Datta, T. E. Bell and L. Torrente-Murciano, *Top. Catal.*, 2019, **62**, 1169–1177.
7 J. El-Kadi, K. V. Kinhal, L. Liedtke, J. L. Pinzón-Ramírez, C. Smith and L. Torrente-Murciano, *Philos. Trans. R. Soc., A*, 2024, **382**, 17.
8 C. Smith and L. Torrente-Murciano, *Nat. Chem. Eng.*, 2025, **2**, 261–272.
9 International Energy Agency, *The future of hydrogen, seizing today's opportunities. Report prepared by the IEA for the G20, Japan*, Paris, France, 2019.
10 N. A. Hussein, A. Valera-Medina and A. S. Alsaegh, *Energy Procedia*, 2019, **158**, 2305–2310.
11 D. A. Hansgen, D. G. Vlachos and J. G. Chen, *Nat. Chem.*, 2010, **2**, 484–489.
12 C. J. H. Jacobsen, S. Dahl, P. L. Hansen, E. Tornqvist, L. Jensen, H. Topsoe, D. V. Prip, P. B. Moenshaug and I. Chorkendorff, *J. Mol. Catal. A: Chem.*, 2000, **163**, 19–26.
13 K. Honkala, A. Hellman, I. N. Remediakis, A. Logadottir, A. Carlsson, S. Dahl, C. H. Christensen and J. K. Nørskov, *Science*, 2005, **307**, 555–558.
14 J. Gavnholt and J. Schiøtz, *Phys. Rev. B: Condens. Matter Mater. Phys.*, 2008, **77**, 035404.
15 L. Wang, Y. Zhao, C. Y. Liu, W. M. Gong and H. C. Guo, *Chem. Commun.*, 2013, **49**, 3787–3789.
16 M. Bradford, P. Fanning and M. Vannice, *J. Catal.*, 1997, **172**, 479–484.
17 W. Q. Zheng, J. Zhang, B. Zhu, R. Blume, Y. L. Zhang, K. Schlichte, R. Schlogl, F. Schuth and D. S. Su, *ChemSusChem*, 2010, **3**, 226–230.
18 F. R. Garcia-Garcia, A. Guerrero-Ruiz and I. Rodriguez-Ramos, *Top. Catal.*, 2009, **52**, 758–764.
19 W. Q. Zheng, J. Zhang, H. Y. Xu and W. Z. Li, *Catal. Lett.*, 2007, **119**, 311–318.
20 W. I. F. David, G. D. Agnew, R. Bañares-Alcántara, J. Barth, J. B. Hansen, P. Bréquigny, M. de Joannon, S. F. Stott, C. F. Stott, A. Guati-Rojo, M. Hatzell, D. R. Macfarlane, J. W. Makepeace, E. Mastorakos, F. Mauss, A. Medford, C. Mounaim-Rousselle, D. A. Nowicki, M. A. Picciani, R. S. Postma, K. H. R. Rouwenhorst, P. Sabia, N. Salmon, A. N. Simonov, C. Smith, L. Torrente-Murciano and A. Valera-Medina, *JPhys Energy*, 2024, **6**, 56.
21 T. E. Bell and L. Torrente-Murciano, *Top. Catal.*, 2016, **59**, 1438–1457.
22 P. Munnik, P. E. de Jongh and K. P. de Jong, *Chem. Rev.*, 2015, **115**, 6687–6718.
23 S. Cattaneo, S. Althahban, S. J. Freakley, M. Sankar, T. Davies, Q. He, N. Dimitratos, C. J. Kiely and G. J. Hutchings, *Nanoscale*, 2019, **11**, 8247–8259.
24 J. Ran, X. Wang, Y. Liu, S. Yin, S. Li and L. Zhang, *Mater. Horiz.*, 2023, **10**, 2343–2372.
25 J. F. Reynes, F. Leon and F. García, *ACS Org. Inorg. Au*, 2024, **4**, 432–470.
26 N. M. Alyami, A. P. LaGrow, D. H. Anjum, C. Guan, X. Miao, L. Sinatra, D.-J. Yuan, O. F. Mohammed, K.-W. Huang and O. M. Bakr, *Cryst. Growth Des.*, 2018, **18**, 1509–1516.
27 N. Chakroune, G. Viau, S. Ammar, L. Poul, D. Veautier, M. M. Chehimi, C. Mangeney, F. Villain and F. Fiévet, *Langmuir*, 2005, **21**, 6788–6796.
28 J. Yang, T. C. Deivaraj, H.-P. Too and J. Y. Lee, *Langmuir*, 2004, **20**, 4241–4245.
29 X. Yan, H. Liu and K. Y. Liew, *J. Mater. Chem.*, 2001, **11**, 3387–3391.
30 R. Axet and K. Philippot, *Chem. Rev.*, 2020, **120**, 1085–1145.
31 I. L. Simakova, Y. S. Demidova, E. V. Murzina, A. Aho and D. Y. Murzin, *Catal. Lett.*, 2016, **146**, 1291–1299.
32 K. J. Wu and L. Torrente-Murciano, *React. Chem. Eng.*, 2018, **3**, 267–276.
33 B. Pinho and L. Torrente-Murciano, *Adv. Energy Mater.*, 2021, **11**, 2003885.
34 Y. Gao, *PhD Thesis*, University of Cambridge, 2021.
35 J. El-Kadi, E. Fenoaltea Pieche, S. W. Ko and L. Torrente-Murciano, *React. Chem. Eng.*, 2024, **9**, 1145–1153.
36 L. Torrente-Murciano, A. Gilbank, B. Puertolas, T. Garcia, B. Solsona and D. Chadwick, *Appl. Catal., B*, 2013, **132–133**, 116–122.
37 S. Agarwal and J. N. Ganguli, *RSC Adv.*, 2014, **4**, 11893–11898.
38 Q. Zhang, K. Kusada, D. Wu, T. Yamamoto, T. Toriyama, S. Matsumura, S. Kawaguchi, Y. Kubota and H. Kitagawa, *Nat. Commun.*, 2018, **9**, 510.

39 T. Suoranta, M. Niemelä and P. Perämäki, *Talanta*, 2014, **119**, 425–429.
40 A. K. Hill and L. Torrente-Murciano, *Int. J. Hydrogen Energy*, 2014, **39**, 7646–7654.
41 B. Lin, Y. Liu, L. Heng, X. Wang, J. Ni, J. Lin and L. Jiang, *Ind. Eng. Chem. Res.*, 2018, **57**, 9127–9135.
42 J. Lin, L. Zhang, Z. Wang, J. Ni, R. Wang and K. Wei, *J. Mol. Catal. A: Chem.*, 2013, **366**, 375–379.
43 T. Bell, H. Ménard, J. González Carballo, R. Tooze and L. Torrente-Murciano, *Int. J. Hydrogen Energy*, 2020, **45**, 27210–27220.
44 L. Torrente-Murciano, *J. Nanopart. Res.*, 2016, **18**, 87.
45 S. Armenise, F. Cazaña, A. Monzón and E. García-Bordejé, *Fuel*, 2018, **233**, 851–859.
46 A. M. Karim, V. Prasad, G. Mpourmpakis, W. W. Lonergan, A. I. Frenkel, J. G. G. Chen and D. G. Vlachos, *J. Am. Chem. Soc.*, 2009, **131**, 12230–12239.
47 A. Navrotsky, C. Ma, K. Lilova and N. Birkner, *Science*, 2010, **330**, 199–201.
48 N. W. Hurst, S. J. Gentry, A. Jones and B. D. McNicol, *Catal. Rev.: Sci. Eng.*, 1982, **24**, 233–309.
49 N. Araki, K. Kusada, S. Yoshioka, T. Sugiyama, T. Ina and H. Kitagawa, *Chem. Lett.*, 2019, **48**, 1062–1064.
50 K. Kusada, H. Kobayashi, T. Yamamoto, S. Matsumura, N. Sumi, K. Sato, K. Nagaoka, Y. Kubota and H. Kitagawa, *J. Am. Chem. Soc.*, 2013, **135**, 5493–5496.
51 A. C. Bueno, M. Mayer, M. Weber, M. Bechelany, M. Klotz and D. Farrusseng, *Catalysts*, 2019, **9**, 577.